



HAL
open science

Local study of the corrosion kinetics of hardened Portland cement under acid attack

Heloise Gay, Thomas Meynet, Jean Colombani

► **To cite this version:**

Heloise Gay, Thomas Meynet, Jean Colombani. Local study of the corrosion kinetics of hardened Portland cement under acid attack. *Cement and Concrete Research*, 2016, 90, pp.36-42. 10.1016/j.cemconres.2016.09.007 . hal-02303925

HAL Id: hal-02303925

<https://univ-lyon1.hal.science/hal-02303925>

Submitted on 21 May 2021

HAL is a multi-disciplinary open access archive for the deposit and dissemination of scientific research documents, whether they are published or not. The documents may come from teaching and research institutions in France or abroad, or from public or private research centers.

L'archive ouverte pluridisciplinaire **HAL**, est destinée au dépôt et à la diffusion de documents scientifiques de niveau recherche, publiés ou non, émanant des établissements d'enseignement et de recherche français ou étrangers, des laboratoires publics ou privés.

Local study of the corrosion kinetics of hardened Portland cement under acid attack

Héloïse Gay, Thomas Meynet, Jean Colombani

*Institut Lumière Matière; Université de Lyon; Université Claude Bernard Lyon 1;
CNRS, UMR 5306; Domaine scientifique de la Doua, F-69622 Villeurbanne cedex,
France*

Abstract

Whereas the chemical reactions occurring during the acid corrosion of cementitious materials are now well known, their reaction rate have still not been measured. We propose here a methodology using digital holographic interferometry to access to the pure surface reaction rate. This method makes possible the differentiation between the dissolution and precipitation steps. We use it to measure the reaction rate constant of the dissolution of hardened Portland cement in aqueous solutions of nitric, sulfuric and hydrochloric acid at pH 2. This quantity is seen to be unexpectedly similar for the three acids, with a value of the order of 1 mg/m²/s. We have measured the evolution of this reaction rate constant with the pH in nitric acid. We have also measured the real pH of the solution at the material surface, which is always alkaline (pH>11), even for attacks by solution with pH as low as 1.

Keywords: A: reaction, A: kinetics, A: pH, C: corrosion, acid

1. Introduction

2 The extension of the durability of concrete buildings necessitates the
3 understanding of its limiting factors, like creep, crack propagation by water
4 freezing, degradation due to aggressive environments, etc. Among chemi-
5 cal attacks reducing the service life of construction materials, acid attack is
6 particularly detrimental to materials as alkaline as cementitious materials.

Email address: Jean.Colombani@univ-lyon1.fr (Jean Colombani)

7 Indeed the hydration products of cement are neutralized by protons, induc-
8 ing dissolution and precipitation of new salts, destroying the microstructure
9 of this hydraulic binder. The mechanisms of action of acid reagents on con-
10 crete, mainly originating outdoor in air pollution (dry deposition) and acid
11 rains (wet deposition), have been investigated for a few decades, and the
12 basic features are now identified [1, 2, 3]. These modes of action have also
13 been studied indoor in the case of industrial constructions involving acidic
14 environments [4, 5]. These mechanisms, including heterogeneous reactions,
15 ion substitution, mass loss, diffusion of solution in pores, strain, porosity
16 evolution, leaching, etc. are complex, interact with each other, and lead to
17 a loss of strength and stiffness of the material.

18 The investigation of acid attack on cement-based materials has been
19 performed either with field measurements in urban areas [6, 7], or with
20 laboratory measurements. The latter have used either simulated acid rain
21 solutions [7, 8, 9], or concentrated acid aqueous solutions [10], in order to
22 accelerate the reactions. Sometimes, different reagents are tested simultane-
23 ously or alternatively [10, 4]. In the course of these studies, three parameters
24 are generally evaluated: the chemical composition of the runoff solution, the
25 change of mass or size of the samples, and their strength decrease. Due to
26 the complexity of the phenomenon, a quantity is generally not measured, al-
27 though being the fundamental parameter of chemical kinetics: the reaction
28 rate.

29 Up to now, models of degradation of concrete under acid attack use em-
30 pirical dissolution laws [11]. We think that the knowledge of well-defined
31 reaction parameters may help in the elaboration of the predicting tools of
32 acid corrosion. As the reaction of dissolution is always combined with other
33 phenomena like precipitation, flow of the solution, diffusion of dissolved
34 species, etc. in standard acid attack setups, these experiments are not us-
35 able for pure corrosion rate measurement. Therefore we propose in this
36 article an original methodology, using holographic interferometry, to access
37 to the reaction rate of cementitious materials in acid solutions. We provide
38 values of the pure dissolution rate of hardened Portland cement in three
39 strong acids —nitric, sulfuric and hydrochloric acids— at various pH as first
40 examples of measurements.

41 Our investigation of hydrated cement acid attack follows a non-conventional
42 procedure, focusing on one single step of the phenomenon, namely on the
43 first one, dissolution. Accordingly a comparison of our results with standard
44 studies on the resistance of cement-based materials to acid is not directly
45 possible [12]. Indeed these experiments are global ones, including dissolu-
46 tion, precipitation, cracking, volume expansion ... and do not enable to

CaO	SiO ₂	Al ₂ O ₃	Fe ₂ O ₃	Na ₂ O	MgO	K ₂ O	SO ₂
62.7	17.7	5.5	4.1	0.4	0.8	0.7	3.7

Table 1: Composition (mass %) of the ordinary Portland cement used in the corrosion experiments.

47 isolate pure dissolution. But we hope that our main results —values of the
 48 reaction rates, real value of the pH at the attacked surface, evidence of the
 49 tiny influence of the nature of the strong acid— will (i) find verification in
 50 standard studies, and (ii) help to model more accurately acid degradation
 51 of cementitious materials.

52 **2. Materials and method**

53 *2.1. Samples and acidic solutions*

54 We have used in this study ordinary Portland cement (CEM-1), the
 55 composition of which is detailed in table 1. It is made of at least 95%
 56 clinker. The cement paste was cast in Petri dishes and cut, after 28 days of
 57 curing in a moist environment, in order to obtain parallelepipedic samples
 58 of approximate dimensions $5 \times 5 \times 0.5$ mm³. The water over cement ratio
 59 was 0.4. The nitric, sulfuric and hydrochloric acid solutions were diluted
 60 with pure water to obtain the required pH. These three inorganic acids
 61 being strong, the pH is the convenient quantity to indicate the content of
 62 aggressive species in solution. All experiments have been carried out at
 63 ambient temperature.

64 *2.2. Holographic interferometry*

65 Our final aim is the measurement of a reliable reaction rate of hardened
 66 cement in acid solutions. To be unquestionable, the experiments must guar-
 67 antee that no other phenomenon (convection, precipitation . . .) disturbs the
 68 measurement, to provide a pure dissolution rate. This implies that, during
 69 the acid attack of the samples, we are able (i) to observe the interface where
 70 the reaction proceeds, to study the reaction precisely where it occurs, and
 71 (ii) to access to the concentration field in the liquid soaking the solid, in
 72 order to detect all possible mass transport phenomena (diffusion, convec-
 73 tion) and remove their contribution from the reaction rate. To achieve these
 74 two goals, we have carried out real-time digital holographic interferometry
 75 measurements.

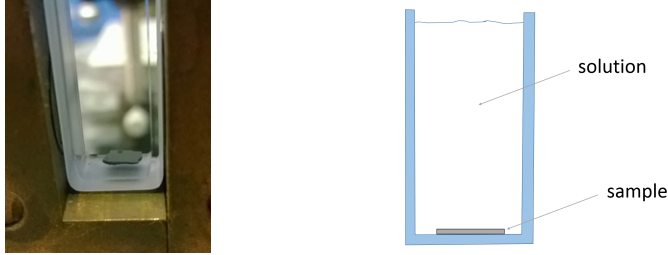


Figure 1: Photograph and diagram of the experimental cell, containing the acid solution and the hardened cement sample at the bottom.

76 Here we take advantage of the potentiality of holography to record phase
 77 objects, i.e., transparent objects exhibiting only variation of their index of
 78 refraction in our case. Here the investigated transparent object is the solu-
 79 tion where the solid dissolves, contained in a transparent cell of dimensions
 80 $10 \times 10 \times 40 \text{ mm}^3$ (figure 1). We record first the state of this corrosive
 81 liquid in a so-called reference digital hologram at time t_0 . Here, we choose
 82 for t_0 the moment just before the solid is introduced in the cell. Then the
 83 hardened cement thin sample is placed at the bottom of the cell. Subse-
 84 quently we record periodically the digital hologram of the liquid during the
 85 attack of the solid. Afterwards we perform numerically a superposition of
 86 the holograms at time t_0 and at the various times t to obtain interferograms
 87 of the evolution of the state of the liquid between times t_0 and t (figure 2).
 88 The evolution of the concentration c in the solution, due to the ion release
 89 stemming from the attack, induces a change of the refractive index, hence
 90 of the phase of the liquid, which is visualized through interference fringes.
 91 We want to emphasize that holographic interferometry differentiates from
 92 classical interferometry in the fact that no external reference is needed, the
 93 object interfering virtually with a memory of itself [13].

94 A numerical procedure enables to reconstruct the two-dimensional con-
 95 centration field in the liquid from the fringes (figure 3). As only concentra-
 96 tion changes inside the cell here, and the concentration was initially uniform,
 97 interference fringes are iso-concentration curves. The fringes have always
 98 been observed horizontal, so we can deduce that concentration is horizon-
 99 tally invariant, and the evolution is only one-dimensional, in the vertical
 100 direction.

101 The chemical reaction is considered first-order, with the dissolution flux
 102 at the interface writing $J = ks_r(1 - c/s)$ with k the reaction rate constant,
 103 s_r the reactive surface area, c the concentration of the dissolved species and

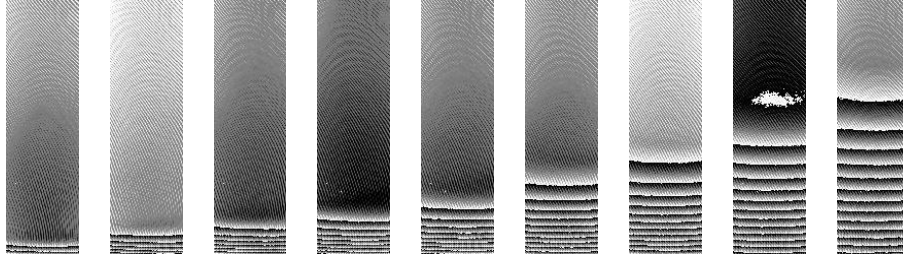


Figure 2: Digital holographic interferograms of the dissolution of a hardened Portland cement sample at the bottom of a nitric acid solution of pH 1.5, at 5, 15, 30, 50, 80, 130, 220, 400 and 600 min after the introduction of the sample at the bottom of the cell. The dimension of each interferogram is $5 \times 18 \text{ mm}^2$.

104 s their solubility limit. The two physico-chemical quantities s and k both
 105 depend on the thermodynamic conditions, the sole varying parameter of
 106 which here is the pH. The reaction rate J can be viewed as the velocity with
 107 which the concentration curve at the interface $z = 0$ shifts upward (figure
 108 3).

The solution of Fick's second law with this chemical reaction at the solid-liquid interface, in a semi-infinite one-dimensional approximation, brings the theoretical concentration evolution $c(z, t)$ with vertical dimension z and time t in the cell:

$$c(z, t) = s \left[\operatorname{erfc} \left(\frac{z}{2\sqrt{Dt}} \right) - \exp \left[\frac{k(s_r/s_d)z}{D\rho s} + \left(\frac{k(s_r/s_d)}{D\rho s} \right)^2 Dt \right] \times \operatorname{erfc} \left[\frac{z}{2\sqrt{Dt}} + \frac{k(s_r/s_d)}{D\rho s} \sqrt{Dt} \right] \right] \quad (1)$$

109 with s_d the section of the experimental cell, ρ the density of the solution,
 110 and D the diffusion coefficient of the dissolved species. The best fit of the
 111 experimental curves deduced from the holographic results with the analytic
 112 expression of $c(z, t)$ brings the pure surface reaction rate constant k , the
 113 solubility of the dissolved species s , and their mean diffusion coefficient D
 114 (figure 3).

115 We stress on the fact that the solubility s measured here is the saturation
 116 concentration of the dissolving components of hardened cement (see section
 117 3 for the nature of these components). This solubility has no link with the
 118 components precipitating later in the course of the experiment.

119 Details on the experimental device and data analysis have been given
 120 elsewhere, applied to the situation of gypsum dissolution in water [14] and

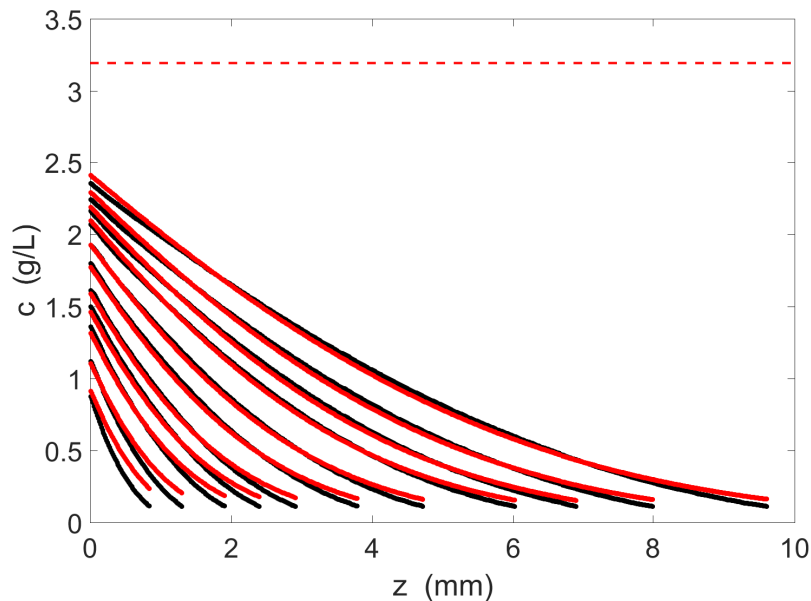


Figure 3: Experimental (black curves) and theoretical (red curves) concentration of dissolved cement hydrate in a nitric acid solution of pH 1.5 versus vertical dimension. The curves correspond to the times 9, 15, 25, 35, 47, 70, 100, 150, 190, 250 and 350 min of the experiment. The horizontal line is the extrapolated saturation concentration s of the dissolved species. The sample lies at $z = 0$.

121 in various aqueous solutions [15].

122 This method of investigation of hydrated cement corrosion by acid solu-
 123 tions brings the following advantages:

- 124 1. The observation of the two-dimensional concentration field in the liq-
 125 uid enables to state that the mass transport of the dissolved species
 126 in our quiescent liquid is exclusively diffusional, thereby validating the
 127 use of Fick's law to determine the theoretical concentration profile.
 128 Indeed, the presence of any non-diffusive fluxes (natural convection,
 129 gravitational instability ...) would have induced a distortion of the
 130 interference fringes [16].
- 131 2. After a first step of pure dissolution, precipitation of salts stemming
 132 from the neutralization of the mineral occurs [1]. The pure dissolu-
 133 tion rate can be estimated from the concentration curves only before
 134 this recrystallisation sets in. The holographic interferometry offers

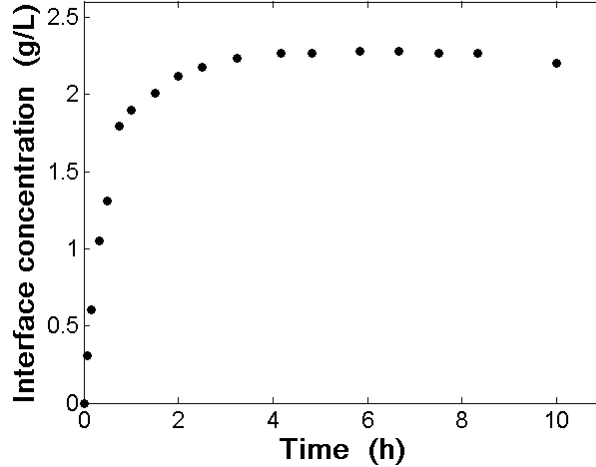


Figure 4: Evolution with time of the concentration of dissolved hardened cement at the solid-liquid interface $z = 0$ during the dissolution of a hardened Portland cement sample at the bottom of a nitric acid solution of pH 1.5.

135 the chance to follow the concentration at the solid-liquid interface
 136 $c(z = 0, t)$. In figure 3, this value can be read at the ordinate axis. It
 137 evolves upward due to the matter release caused by the attack. Precipitation
 138 consumes ions and thereby induces a decrease of the interface
 139 concentration. Therefore, as soon as $c(z = 0, t)$ decreases, the corre-
 140 sponding concentration curves are excluded from the fitting, to assure
 141 that only dissolution is taken into account. An example of concentra-
 142 tion evolution with time at the interface during dissolution is shown in
 143 figure 4. In this case, the curves have been taken into account for the
 144 computation of the reaction rate constant only before the beginning
 145 of the plateau, at time $t \simeq 4$ h.

- 146 3. The good agreement between the experimental curves and the theo-
 147 retical law constitutes a validation of our assumption that what occurs
 148 is a pure dissolution phenomenon with a first-order reaction.

149 2.3. Refractive index of the solution

150 The holographic interferometry device provides a two-dimensional phase
 151 map $\phi(y, z)$. The transformation of the phase into concentration has two
 152 requirements. First, the concentration must be known in each interferogram

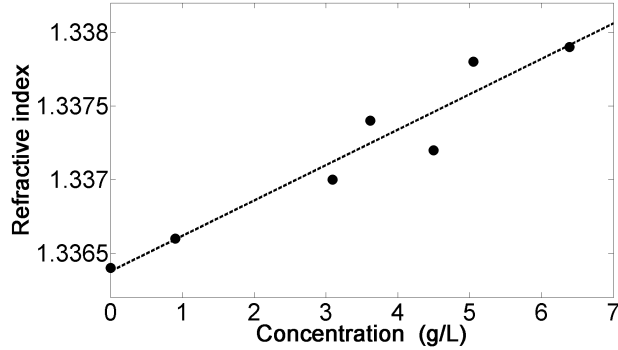


Figure 5: Index of refraction of an aqueous solution of nitric acid of pH 1 *vs* concentration of dissolved hardened Portland cement. The line is a linear fit.

153 at least in one point, the rest of the absolute concentration field being de-
 154 duced by comparison with this point. As the initial liquid is the pure acid
 155 aqueous solution, free from dissolved matter, the concentration at the top
 156 of the cell is always $c = 0$. This is always true because, during the course
 157 of our experiments, we pay attention to the fact that no fringe has the
 158 time to reach the top of the cell. Secondly, the concentration is computed
 159 from the phase ϕ via the formula $c = \lambda\phi/[2\pi e(\partial n/\partial c)]$, where λ is the laser
 160 wavelength ($\lambda = 532$ nm), e the depth of the cell ($e = 10$ mm) and n the
 161 refractive index of the solution. The variation of the index of refraction of
 162 the solution with the concentration of dissolved species $\partial n/\partial c$ is therefore a
 163 crucial parameter. To gain this value, we have dissolved various quantities
 164 precisely weighed of finely ground hardened cement in pure aqueous solution
 165 of nitric acid of pH 1. Then we have measured the refractive index of this
 166 solution with an Abbe refractometer (figure 5). The slope of the $n(c)$ curve
 167 is the searched parameter $\partial n/\partial c = 2.4 \times 10^{-4}$ L/g.

168 We have measured the reaction rate of hydrated cement under acid at-
 169 tack at different pH. So to estimate the influence of pH on $\partial n/\partial c$, the refrac-
 170 tive index of an aqueous solution of pure nitric acid for various pH has been
 171 measured with the Abbe refractometer. It can be seen in figure 6 that the
 172 index of refraction is constant, except for very small pH, where it increases
 173 of 0.2%. In these conditions, we have estimated that the influence of the pH
 174 on $\partial n/\partial c$ is negligible.

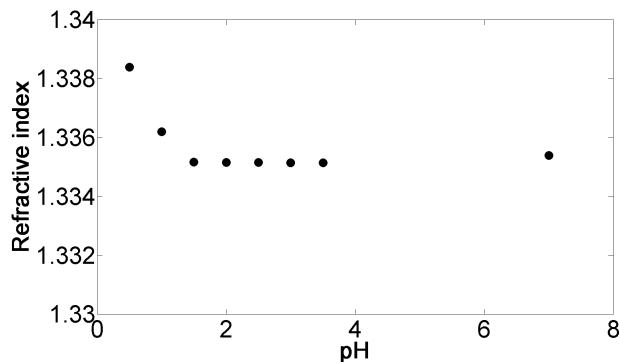
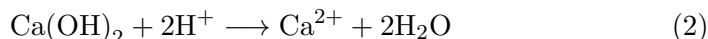


Figure 6: Index of refraction *vs* pH of an aqueous solution of nitric acid.

175 3. Reactions during acid attack

176 Sulfuric, hydrochloric and nitric acids have been chosen because they are
 177 ones of the main acidic components in acid rains [6]. The chemical reactions
 178 of hydrated cement in these acid solutions have already been studied in
 179 detail. As our aim is not to discuss these reactions but to measure their
 180 kinetics, we will just recall them briefly. Under acid pH, all the constituents
 181 (calcium hydroxides, calcium silicate hydrates (CSH), calcium aluminate
 182 hydrates (CAH) . . .) dissolve at various velocities, and new salts precipitate.
 183 The first and faster dissolving component is calcium hydroxide –also called
 184 Portlandite– along the neutralization reactions [7]:



185 The nature of the calcium salts crystallizing subsequently depend on the
 186 anion provided by the acid, typically gypsum and ettringite in the case of
 187 sulfuric acid. The severity of the attack is considered to be mainly dependent
 188 on the solubility of the precipitated salts. Indeed in the case of highly insol-
 189 uble salts, e.g. fluoride salts, a dense layer forms at the interface, protecting
 190 the material [2]. But to try to understand more clearly the mechanisms at
 191 the beginning of the attack, we have restricted ourselves in this study to the
 192 first stage of the acid attack, where the main phenomenon is the dissolution
 193 of Portlandite, and we have not studied the subsequent precipitation of pos-
 194 sibly protecting layers. Therefore we access here to the pure severity of the
 195 acid attack, whatever the further reactions.

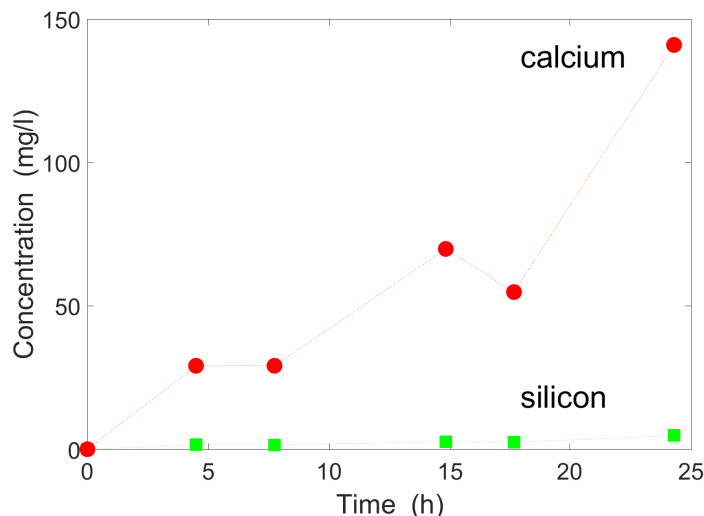


Figure 7: Concentration of dissolved calcium (red circles) and silicon (green squares) as a function of time during the attack of hardened Portland cement by quiescent nitric acid at $\text{pH} = 2$, measured with ICPAES.

196 To assess that the reaction scenario is really the above-mentioned one,
 197 we have performed additional chemical analyses of the attacked surface and
 198 of the soaking solution. The surface measurements have been carried out
 199 with the energy dispersive X-ray spectrometer (EDS) of a scanning electron
 200 microscope (SEM) and have brought the *post mortem* concentration of the
 201 main elements (Si, Ca, Al, Na, Mg, K, Ti, Mn, Fe) at the hardened cement
 202 surface after various attack durations. The solution measurements have
 203 been achieved with induced coupled plasma atomic emission spectroscopy
 204 (ICPAES) and enabled to access to the silicon, aluminum and calcium con-
 205 centrations in the solvent after some attack durations. The solution has been
 206 stirred before sampling to guarantee the homogeneity of the concentrations.

207 The evolution with time of the calcium and silicon concentration in the
 208 attacking solution during an experiment is shown in figure 7. Besides, the
 209 time change of the concentration of calcium and silicon at the surface of
 210 the attacked hardened cement during the same experiment are presented in
 211 figure 8. The calcium concentration is seen to decrease at the solid surface
 212 and to increase in the liquid. Oppositely, the silicon concentration increases
 213 slowly at the surface and remains almost zero in the solution. These four

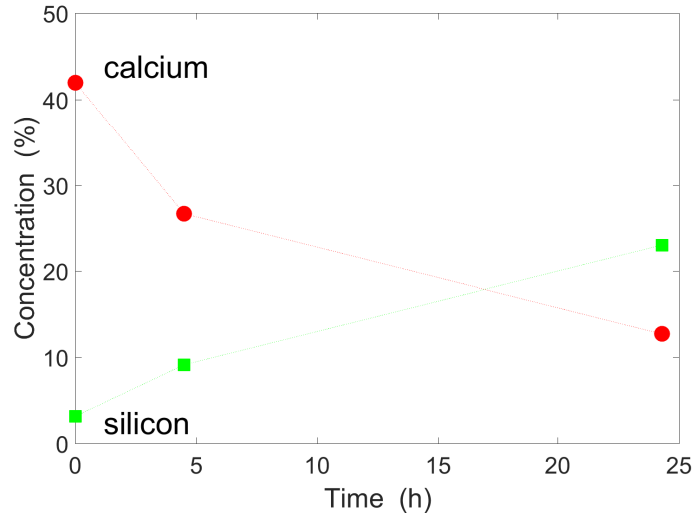


Figure 8: Concentration of calcium and silicon atoms (in percentage of total elements) vs time at the surface of the attacked hardened cement of figure 7, measured with SEM EDS.

214 features are in perfect agreement with the above-explained expected attack
 215 mechanism. The fastest dissolving component is Portlandite, so calcium
 216 atoms progressively disappear from the surface and calcium ions are released
 217 in the acid solution. On the other side, CSH dissolves orders of magnitude
 218 slower than Portlandite and the release of silicon ions in the solution is al-
 219 most negligible during the course of our experiment. As surface Portlandite
 220 fade away, CSH is uncovered and the concentration of silicon at the very
 221 surface increases.

222 Except aluminum, the concentration of all other elements at the attacked
 223 surface is 1% or below during the experiment. The surface concentration
 224 of aluminum is 5% and remains constant during the attack duration. The
 225 concentration of aluminum in the solution during the experiment is always
 226 about 1 mg/l, close to the measurement uncertainty. These results show
 227 that CAH, like CSH, is not affected by the attack for the duration of our
 228 experiment.

229 We wish to finish this section about the chemical reactions during the
 230 attack by mentioning that we have omitted a fundamental aspect of the
 231 reaction. Indeed the heterogeneous and evolving nature of the reactive sur-

232 face has been observed to be highly influential on the reaction kinetics of
233 minerals [17]. But as nothing has been measured yet in hardened cement
234 attacked by acid concerning the possible disparities of reaction kinetics of
235 individual components, we have considered a constant and uniform reactive
236 surface area, which has enabled to fit perfectly the experimental concentra-
237 tion curves.

238 **4. Validation of the holographic procedure**

239 As measurements of pure reaction rates had not been performed up to
240 now, the comparison of our values with other ones, in order to validate them,
241 is not possible for the moment. Indeed, existing studies usually present over-
242 all matter loss, including dissolution, precipitation and mass transfer in the
243 solution and inside the porous solid. Therefore the comparison with mate-
244 rial loss by pure dissolution is not directly possible. But to enable a future
245 possible link with standard studies of acidic attack of cement-based materi-
246 als, we have measured the mass loss of our samples during the experiments.
247 To do so, we have dried the attacked platelets at 100°C during 2 h, then
248 weighed them. From this and their initial mass, we have computed their
249 mass loss due to the acid attack. Beside, we have estimated this mass loss
250 from the numerical integration of the holographic concentration curve at the
251 last investigated time (just preceding precipitation). As seen in figure 9, the
252 measured and computed values of the mass loss compare well, thus validat-
253 ing the holographic procedure. This check attests that the total quantity of
254 damaged material can then be deduced from the holographic measurements.

255 To further assess the accuracy of the holographic method, we have also
256 compared the evolution of the quantity of dissolved calcium during the at-
257 tack, as measured by ICPAES, with the evolution deduced from the nu-
258 merical integration of the concentration curves measured by holointerfer-
259 ometry, considering that only Portlandite dissolves. As seen in figure 10,
260 both evolutions compare well, the holographic measurements reflect quite
261 quantitatively the progressive release of ions in the solution.

262 These two agreements between holography and standard measurements
263 validate our methodology and our measured reaction rate constants.

264 **5. Holographic results**

265 Figure 11 displays the evolution of the solubility limit of hardened Port-
266 land cement in a pure aqueous solution of nitric acid for various pH obtained
267 by holointerferometry. The quantities of matter are expressed as moles of

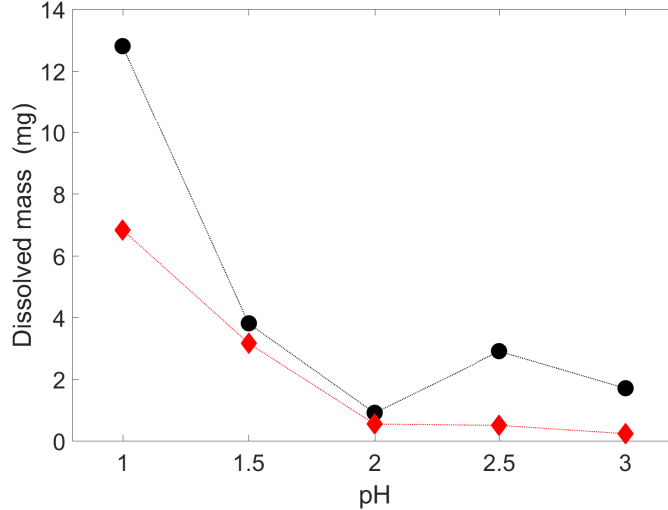


Figure 9: Mass of hydrated cement dissolved in nitric acid at the end the holographic experiment as a function of pH: measured mass (black circles) and estimated mass from the holographic measurements (red diamonds).

268 Portlandite (molar mass $M = 74$ g/mol), the latter being the only con-
 269 stituent contributing significantly to dissolution (section 3).

270 As our measurements are nonstandard ones, we first detail the signifi-
 271 cation of the found solubilities. If Portlandite is considered to be in ex-
 272 cess, the saturation calcium concentration and pH should be fixed by the
 273 solubility product K_s of the reaction $\text{Ca}(\text{OH})_2 \rightarrow \text{Ca}^{2+} + 2\text{OH}^-$. As
 274 $K_s = [\text{Ca}^{2+}]_{\text{sat}}[\text{OH}^-]_{\text{sat}}^2 = 10^{-5.435}$ and the reaction releases at the same
 275 time one calcium and two hydroxide ions, the saturation calcium concentra-
 276 tion is $s = [\text{Ca}^{2+}]_{\text{sat}} = (K_s/4)^{1/3} = 10$ mmol/L and the final pH is 12.3. We
 277 have added this solubility of calcium in figure 11 as a dashed line. We see
 278 that, from pH 2 on, the saturation concentration of the hardened cement
 279 corresponds to the one of Portlandite in the case where the pH is freely fixed
 280 by the reaction equilibrium.

281 We want to stress on the fact that this solubility s is the saturation
 282 concentration of calcium in equilibrium exclusively with solid Portlandite,
 283 and does not take into account the solubility of other salts precipitating later
 284 in the experiment. Subsequently nitrate salts precipitate, and the solubility
 285 of calcium is modified accordingly, being in equilibrium with at least two

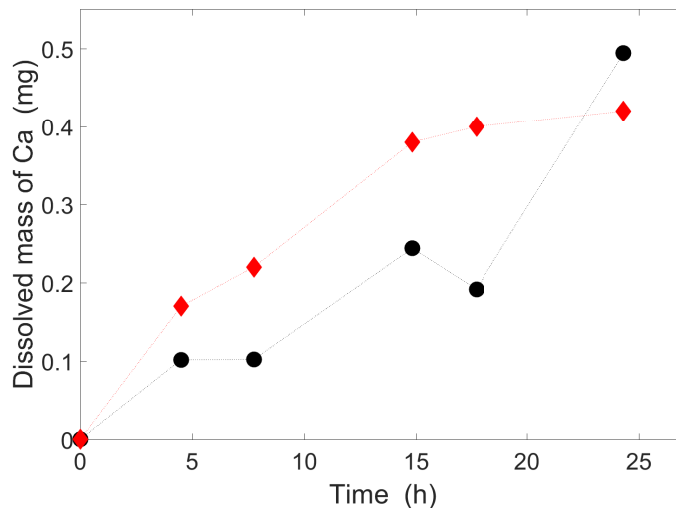


Figure 10: Time evolution of the dissolved calcium mass measured by ICPAES (black circles) and estimated from the holographic measurements (red diamonds) during the attack of hardened cement by nitric acid at $\text{pH} = 2$.

286 solid components (Portlandite and a nitrate salt). For instance in figure 4
 287 the concentrations after 5 h, the time where the calcium concentration starts
 288 to decrease due to precipitation, are excluded from the computation of s ,
 289 which is thereby only characteristic of the Portlandite/solution chemical
 290 equilibrium.

291 Two inferences may be drawn from the nature of the $s(\text{pH})$ curve in
 292 figure 11. First this is a new corroboration of the fact that Portlandite is
 293 here the only dissolving component. Secondly it shows that the pH of the
 294 solution at the interface is not the bulk solution pH , but a pH fixed by the
 295 reaction equilibrium, i.e., $\text{pH}_{\text{surf}} = 14 + \frac{1}{2} \log(K_s/s)$. This surface pH has
 296 been added in figure 11. It is observed to be always very alkaline, higher
 297 than 11, even for a bulk solution pH as low as 1. The interface pH takes
 298 the equilibrium value fixed by the reaction (12.3) for a bulk $\text{pH} \geq 2$. Below
 299 this value, the dissolution kinetics is too fast, compared to the diffusion
 300 kinetics, for the equilibrium value to be kept. Whereas the modification
 301 of the pH of the acidic solution in contact with the solid by the cement
 302 dissolution was expected, the novelty lies in the fact that this pH can be
 303 accurately measured, which enables a precise knowledge of the condition of

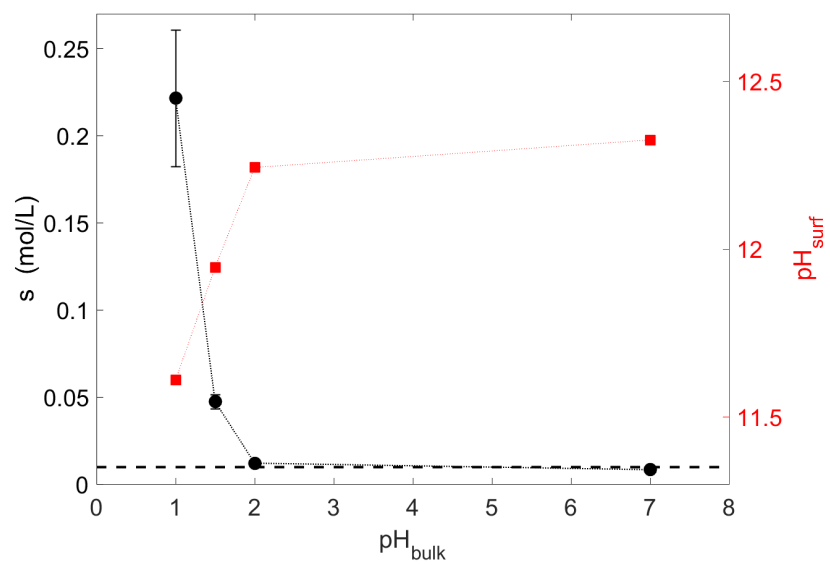


Figure 11: Evolution of the saturation concentration of hardened Portland cement in aqueous solutions of pure nitric acid (black circles) and evolution of the pH at the interface (red squares) with the pH of the bulk solution. The values of concentration are in moles of Portlandite per Liter of solution. The dashed line is the saturation concentration of Portlandite in the case that it freely fixes the final pH.

Acid	k		s	
	(mg/m ² /s)	(mmol/m ² /s)	(g/L)	(mol/L)
Hydrochloric	2.6	0.035	0.9	0.012
Nitric	2.0	0.027	0.9	0.012
Sulfuric	3.1	0.042	1.0	0.014

Table 2: Pure surface reaction rate constant k and solubility of the dissolved hardened cement s for the dissolution of hardened Portland cement in aqueous solutions of various acids for pH = 2. Values are expressed both in mass of dissolved hardened cement and in moles of dissolved Portlandite.

304 the damaging of the cementitious material surface.

305 Figure 12 (top) displays the evolution of the dissolution rate constant of
306 hardened Portland cement in nitric acid as a function of the pH of the bulk
307 solution. Again the quantity of matter is expressed in moles of Portlandite.
308 The bulk pH is the pH of the initial acidic solution, far from the solid-
309 liquid interface. But as has been evidenced in figure 11, the pH close to the
310 interface has been thoroughly modified by the fast release of the OH⁻ due
311 to the reaction. Therefore paradoxically these reaction rate constants are in
312 fact characteristic of the behavior of the material in very alkaline conditions.
313 We have related in figure 12 (bottom) the rate constants to the true pH they
314 are characteristic of.

315 These results may appear puzzling. Indeed to predict the behavior of
316 a cementitious material during an acidic attack at pH 1, the value of the
317 reaction rate constant that should be used is the value at pH 11.5. This is
318 due to the fact that for a heterogeneous reaction, a mass transport boundary
319 layer develops in the vicinity of the solid. When the dissolution flux and the
320 diffusion flux in this layer are of the same order of magnitude (the mixed
321 kinetics regime), both interact and the concentration and the pH at the
322 interface take out of equilibrium values (see a detailed situation in [18]).

323 Table 2 displays the reaction rate constant and saturation concentration
324 of hardened Portland cement in pure aqueous solutions of nitric, sulfuric,
325 and hydrochloric acids at pH = 2. We have expressed the quantities of
326 matter in moles of Portlandite and in grams of hardened cement. As for
327 nitric acid, the solubility of hardened cement in sulfuric and hydrochloric
328 acid corresponds to the solubility of Portlandite free to fix the pH. Therefore
329 the pH of the solution close to the surface for these two acids is likely to be
330 also strongly alkaline, as in figure 11.

331 We see that the behavior of the material is similar in the three acid

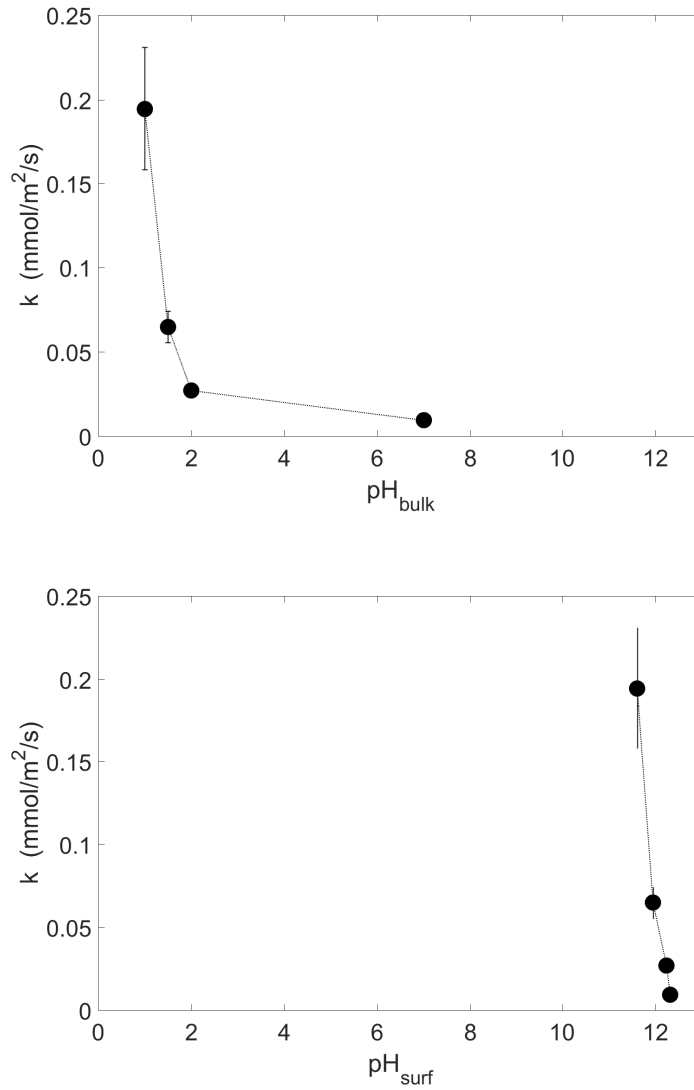


Figure 12: Evolution of the dissolution rate constant of hardened Portland cement in aqueous solutions of pure nitric acid with the bulk pH of the solution (top) and with the surface pH deduced from the local solubility (bottom). The values are in millimoles of Portlandite per unit surface and time.

332 solutions, with values of k ranging within 25% from each other. We would
333 like to emphasize that the fact that the reaction rate constants are highly
334 similar for the three investigated acids is opposite to what is expected from
335 conventional studies [10, 2]. This result demonstrates thus firmly that the
336 kinetics of acid corrosion originates mainly in the precipitation step of the
337 reaction. At this stage, a more or less protective layer progressively covers
338 the surface, modifying the ion detachment rate, whereas before the formation
339 of this layer, the kinetics of all acids are comparable.

340 Finally, we would like also to recall that our method enables to perform
341 a real-time measurement of the spatially resolved reacting system. There-
342 fore, we have been able to discriminate temporally the dissolution from the
343 precipitation. As seen in figure 4, the time before precipitation sets in, i.e.,
344 the time before concentration decreases, is roughly 5 h. This order of mag-
345 nitude has been observed in all our experiments. It gives an idea of the
346 required time before precipitation proceeds in an unstirred acid. It is linked
347 to the time needed for the interface concentration to reach the solubility of
348 the precipitating salts.

349 **6. Implications for hardened cement resistance to acid**

350 As above-recalled, a diffusional boundary layer always builds up over a
351 dissolving solid. In the case of a flowing liquid, this layer shows a thick-
352 ness of the order of tens of μm [18]. In a quiet liquid, the final boundary
353 layer thickness is theoretically infinite. The interface concentration and pH
354 depend on this thickness: the pH will always remain close to 12, and the
355 concentration will range between 0 and $s(\text{pH})$, for instance 0.22 mol/L for
356 pH 1, depending on the relative kinetics of dissolution and diffusion. In
357 the case of acid rain, once the material is wet, it is exposed to a quiescent
358 solution and we are close to the hydrodynamic situation of our experiments.
359 The only difference lies in the geometry, the degradation occurring at the
360 surface and inside the pores, with sizes much smaller than the one of our
361 cell.

362 Contexts in the laboratory and in real buildings being similar, what
363 can we learn from our experiments for future studies? We propose three
364 investigation directions:

- 365 • First, we dispose now of a tool to access the reaction rate of hardened
366 cement in acid. So beside the study of protective layers precipitating
367 after the dissolution step (ettringite . . .), the formulation of materials
368 with low reaction rates can also help to manufacture more durable

369 concrete. Recent measurements of the dissolution rate of hardened
370 cement at alkaline pH show that the Ca/Si ratio can be optimized to
371 lower this rate. This ratio is likely to influence also the kinetics of
372 acidic attack [19].

- 373 • Numerical models of the degradation of concrete in acidic solution
374 make use of empirical laws for the simulation of the dissolution step,
375 rigorous thermochemical parameters being usually not accessible. We
376 have shown here that a nonstandard method can give access to the ex-
377 act reaction kinetics and we think that the integration of such experimen-
378 tally-verified laws inside the models can bring a more realistic repre-
379 sentation of damaging situations. We would like to emphasize that,
380 even when precipitation sets in, the dissolution rate constants that we
381 have measured before this precipitation, are still valid, being thermo-
382 dynamically characteristic of the kinetics of the dissolution.
- 383 • At last, for industrial situations with harsh acid conditions, where the
384 material is for instance exposed to a long-lasting acidic attack, cement-
385 based materials have to be adapted to this stringent environment. In
386 this case, the introduction in the formulation of admixtures known
387 for their strong adsorption at the hardened cement surface, related to
388 their calcium-complexing nature, could help lowering the dissolution
389 rate of Portlandite in acid. Moreover it is likely that already used
390 admixtures, like superplasticizers, play such a role in adsorbing at the
391 $\text{Ca}(\text{OH})_2$ surface. The optimization of their conformation, with the
392 aim of reducing k may lead to more durable materials.

393 7. Conclusion

394 We have introduced in this article a methodology, including holographic
395 interferometry, that gives access to the space and time resolution of hetero-
396 geneous reactions. In the case of the study of the degradation of hydrated
397 cement, it enables to clearly discriminate between the dissolution and precip-
398 itation stages of the deterioration. This technique has been used to measure
399 the dissolution rate constant of hardened Portland cement in pure aqueous
400 solutions of hydrochloric, nitric and sulfuric acids at pH 2. Unexpectedly,
401 the three values have been found to compare well, about $1 \text{ mg/m}^2/\text{s}$. This
402 is a direct demonstration that the degradation kinetics is mostly driven by
403 precipitation. We have also measured the evolution of the reaction rate
404 constant in nitric acid with the pH. Profiting from the resolving power of
405 the technique , we have finally measured accurately the pH of the solution

406 close to the surface, where it has been found to be always strongly alkaline
407 (between 11.5 and 12.5), whatever the bulk pH. Now that ordinary Portland
408 cement has been studied, this technique may be used to test thoroughly the
409 resistance to acid attack of other cementitious materials, known to offer bet-
410 ter acid resistance, like calcium sulfoaluminate cements, or Portland cement
411 containing silica fume.

412 **Acknowledgements**

413 We thank Maurizio Bellotto, Cédric Desroches, Fernand Chassagneux
414 and Susan Stipp for fruitful discussions.

415 **References**

- 416 [1] V. Zivica, A. Bajza, Acidic attack of cement based materials — a
417 review. Part 1. Principle of acidic attack, *Construction and Building*
418 *Materials* 15 (2001) 331.
- 419 [2] V. Zivica, A. Bajza, Acidic attack of cement based materials — a
420 review. Part 2. Factors of rate of acidic attack and protective measures,
421 *Construction and Building Materials* 16 (2002) 215.
- 422 [3] V. Zivica, Acidic attack of cement based materials — a review. Part
423 3. Research and test methods, *Construction and Building Materials* 18
424 (2004) 683.
- 425 [4] F. Girardi, W. Vaona, R. DiMaggio, Resistance of different types of
426 concretes to cyclic sulfuric acid and sodium sulfate attack, *Cement &*
427 *Concrete Composites* 32 (2010) 595.
- 428 [5] J. Monteny, N. DeBelie, L. Taerwe, Resistance of different types of
429 concrete mixtures to sulfuric acid, *Materials and Structures* 36 (2003)
430 242.
- 431 [6] D. Derry, M. Malati, J. Pullen, Effects of atmospheric acids on Portland
432 cements, *Journal of Chemical Technology and Biotechnology* 76 (2001)
433 1049.
- 434 [7] H. Okochi, H. Kameda, S. Hasegawa, N. Saito, K. Kubota, M. Igawa,
435 Deterioration of concrete structures by acid deposition — an assessment
436 of the role of rainwater on deterioration by laboratory and field exposure
437 experiments using mortar specimens, *Atmospheric Environment* 34
438 (2000) 2937.

- 439 [8] S. Xie, L. Qi, D. Zhou, Investigation of the effects of acid rain on the
440 deterioration of cement concrete using accelerated tests established in
441 laboratory, *Atmospheric Environment* 38 (2004) 4457.
- 442 [9] M. Chen, K. Wang, L. Xie, Deterioration mechanism of cementitious
443 materials under acid rain attack, *Engineering Failure Analysis* 27 (2013)
444 272.
- 445 [10] S. Miyamoto, H. Minagawa, M. Hisada, Deterioration rate of hardened
446 cement caused by high concentrated mixed acid attack, *Construction
447 and Building Materials* 67 (2014) 47.
- 448 [11] R. Beddoe, H. Dorner, Modelling acid attack on concrete: Part i. The
449 essential mechanisms, *Cement and Concrete Research* 35 (2005) 2333.
- 450 [12] V. Zivica, Experimental principles in the research of chemical resistance
451 of cement based materials, *Construction and Building Materials* 12
452 (1998) 365.
- 453 [13] J. Colombani, J. Bert, Holographic interferometry for the study of
454 liquids, *J. Molec. Liquids* 134 (2007) 8.
- 455 [14] J. Colombani, J. Bert, Holographic interferometry study of the disso-
456 lution and diffusion of gypsum in water, *Geochim. Cosmochim. Acta*
457 71 (2007) 1913.
- 458 [15] E. Pachon-Rodriguez, J. Colombani, Pure dissolution kinetics of an-
459 hydrite and gypsum in inhibiting aqueous salt solutions, *AIChE J.* 59
460 (2012) 1622.
- 461 [16] J. Colombani, J. Bert, Holographic convection visualization during
462 thermotransport studies - Application to microgravity experiments,
463 *Meas. Sci. Technol.* 10 (1999) 886.
- 464 [17] C. Fischer, R. Arvidson, A. Luttge, How predictable are dissolution
465 rates of crystalline material?, *Geochim. Cosmochim. Acta* 98 (2012)
466 177.
- 467 [18] J. Colombani, Measurement of the pure dissolution rate constant of a
468 mineral in water, *Geochim. Cosmochim. Acta* 72 (2008) 5634.
- 469 [19] I. Pignatelli, A. Kumar, R. Alizadeh, Y. LePape, , M. Bauchy, G. Sant,
470 Does a dissolution-precipitation mechanism explain concrete creep in
471 moist environments?, *arXiv cond-mat* (2015) 1508.07082.